Physics of the Earth and Planetary Interiors 295 (2019) 106310

Contents lists available at ScienceDirect

Physics of the Earth and Planetary Interiors

journal homepage: www.elsevier.com/locate/pepi

New normal mode constraints on bulk inner core velocities and density

Alexander J.S. Robson[a,*], Barbara Romanowicz[a,b,c]

[a] Earth and Planetary Science, University of California, Berkeley, CA, USA
[b] College de France, Paris, France
[c] Institut de Physique du Globe de Paris, Paris, France

ARTICLE INFO

Keywords:
Inner core
Normal modes
Density jump
Shear velocity
Density

ABSTRACT

Inner core elastic parameters V_p, V_s and density (ρ) inform both experimental and theoretical studies of inner core composition and potential light element candidates. Meanwhile, constraints on the density jump at the inner core boundary offer much-needed observational insight into the processes powering the geodynamo. Thus, obtaining accurate observational constraints on the elastic structure of the inner core is key to gaining better understanding of its composition and dynamics.

While body wave phases provide information on inner core P velocity and anisotropy structure, constraining shear velocity and density currently relies predominantly on core-sensitive normal mode observations. Since the construction of the Preliminary Reference Earth Model (Dziewonski and Anderson, 1981), which was largely based on such data, the database of observed normal modes has become both larger and more accurate, and new model exploration methodologies have become computationally feasible.

Here we use recent normal mode center-frequency catalogues to simultaneously explore average shear (V_s) and compressional (V_p) velocities, as well as density (ρ), in the inner core via a Monte Carlo parameter-space search.

We find best-fitting V_p values (11,160–11,180 m/s) in good agreement with PREM, while V_s values (3560–3590 m/s) favor a minor reduction (< 1% relative to PREM). We show that a recently proposed reduction of 2.5% in V_s in the inner core, while keeping the other two parameters constant, is incompatible with normal mode data, and demonstrate the importance of simultaneously exploring the parameters to address trade-off effects. Meanwhile, we show that ρ is the most poorly-constrained parameter, though mode data without any additional constraints favor a density reduction of ~0.7–1.9% with respect to PREM. We also show that the need for this reduction is largely independent of various assumed parameters, including: the choice of reference mantle and outer core model, observational catalog, and the depth of the ICB.

The presented results may be of interest for laboratory and ab-initio studies aiming at constraining IC composition and for studies that consider the energy available to power the geodynamo via compositional convection.

1. Introduction

Seismological observations are central to our understanding of the Earth's core composition dynamics, and evolution. The fluid core was first discovered using seismic observations in 1906 (Oldham, 1906), by 1936 the existence of an inner-core (IC) was established (Lehmann, 1936), and its solidity finally confirmed in 1970 (Dziewonski and Gilbert, 1971). Meanwhile, Birch established the core's primary composition: an Iron-Nickel alloy (Birch, 1952) with about ~10 wt% light-elements (LE) (Birch, 1964).

It is thought that as the outer core (OC) cools and solidifies, light elements (LEs) partition, preferentially remaining in the fluid (Birch, 1964; Jephcoat and Olson, 1987; Poirier, 1994), leaving the solid IC depleted (~3-5 wt%). The resulting compositional heterogeneity is generally believed to be the driving force for the compositional convection that powers the geodynamo at present (Gubbins et al., 1979; Loper, 1978).

In the years since Birch first proposed the presence of light elements in the earth's core, numerous candidates have been suggested, including Si, O, S, H and C (Antonangeli et al., 2010; Bazhanova et al., 2012; Belonoshko et al., 2007; Caracas, 2015; Hirose et al., 2017; Martorell et al., 2013; Sakamaki et al., 2016; Tagawa et al., 2016; Vočadlo, 2007). However, both ab-initio and laboratory studies have struggled to reconcile these proposed compositions with seismic observations,

* Corresponding author.
E-mail address: a.robson@berkeley.edu (A.J.S. Robson).

https://doi.org/10.1016/j.pepi.2019.106310
Received 14 April 2019; Received in revised form 20 August 2019; Accepted 21 August 2019
Available online 06 September 2019
0031-9201/

consistently recovering incompatibly high velocities, even when matching density (ρ) (Li et al., 2018). This has led to various proposed mechanisms to lower V_s, such as anelasticity, premelting conditions (Martorell et al., 2013) and multiple LEs (Li et al., 2018).

Body wave travel time measurements provide strong constraints on IC V_p, since PKIKP, the inner-core compressional phase, is routinely observed. However, its V_s equivalent, PKJKP, remains elusive. Of five published observations (Cao et al., 2005; Deuss et al., 2000; Julian et al., 1972; Okal and Cansi, 1998; Wookey and Helffrich, 2008), two are thought to be in the wrong frequency band (Deuss et al., 2000), while a recent paper demonstrated the phase may be too low amplitude to observe (Shearer et al., 2011). Body waves provide even less constraint on IC density, though amplitude ratios can provide information on the relative density jump across the ICB. As a result, constraining bulk V_s and ρ in the IC relies primarily on core-sensitive normal mode observations.

The spherically symmetric Preliminary Reference Earth Model (PREM, Dziewonski and Anderson, 1981) was constructed with constraints from normal mode center-frequency measurements, as well as body wave travel times, Earth's mass/moment of inertia, and from the Adams-Williamson equation. PREM is still widely used as a reference for the average V_s, ρ, and quality factors (Qμ and Qκ) in the inner core.

Since PREM was developed, 38 years ago, the database of observed normal mode center-frequencies has grown significantly larger and more accurate, with the addition of data from recent large earthquakes, and theoretical improvements in the measurements, such as including mode splitting and coupling due to 3D structure. Additionally, increases in computation power have made more computationally intensive methodologies accessible.

In the last 20 years, several studies have revisited normal mode constraints on IC density and velocity structure. Masters and Gubbins (2003) used a Backus-Gilbert inversion method to isolate the inner-core density signal, examining bulk IC density, and the density jump (Δρ) across the inner core boundary (ICB). The latter is an important parameter, indicative of the degree of LE partitioning between the IC and the outer core, and thus the energy available to power the geodynamo by such a mechanism.

On the other hand, Deuss (2008) fixed inner core density to that of PREM and searched for the average shear and compressional velocities in the inner core using a grid-search forward modeling scheme, finding average velocities remarkably close to that of PREM when assuming PREM's average density. Another study utilized artificial neural networks (de Wit et al., 2014) to explore normal mode constraints on Earth's 1D structure, though its broad focus and large modal dataset predominantly emphasized sensitivity to mantle structure.

As normal mode studies were consistently finding bulk IC parameters (V_p, V_s and ρ) within 0.5% of PREM (de Wit et al., 2014; Deuss, 2008), an ab-initio study suggested for the first time that these observations could be matched simultaneously, utilizing multiple LE components (Li et al., 2018). However, within months, two papers called bulk core parameters into doubt. A recent Reversible-jump Markov chain Monte Carlo study in the outer core favored a model with increased OC density, drawing into question the robustness of PREM's density structure in the outer core (Irving et al., 2018). Soon after, Tkalčić and Pham (2018) attempted to enhance PKJKP signals using a novel coda-wave correlation technique, proposing that V_s in the IC may be lower than that of PREM by ~2.5%. Yet, their best fitting model appears non-unique, and, as we will show, it does not predict the normal mode center-frequency data better than PREM, in general, and provides very poor fits to several specific modes. Additionally, as with other IC studies (Deuss, 2008), density is kept fixed to that of PREM, in spite of known tradeoffs.

Here, we utilize multiple recent normal mode catalogues, a variety of weighting and error schemes, and computational advances, to better constrain the elastic structure of the IC. We simultaneously explore V_p, V_s, and ρ via a Monte Carlo parameter-space search for models composed of a homogeneous IC (i.e. with no depth dependence), overlain by structure in the OC and mantle, which is fixed to a published 1D background model. We explore multiple background mantle models and discuss the possible influence of mantle and outer core structure on our results.

2. Data

2.1. Catalogues

For this study we consider two sets of observed modal center-frequencies:

- **REM (2001)** a collection of observations from numerous authors and methodologies ("*Reference Earth Model*," n.d.)
- **DR (2013)** observations from Deuss et al. (2013), with the addition of radial mode observations from Roult et al. (2010). Unlike REM, Deuss et al. (2013) accounts for coupling between certain modes and was generated with the addition of data from some recent large events.

2.2. Mode selection

From each of these datasets a subset of IC-sensitive modes were selected. Initially, a list of IC-sensitive modes was compiled from the existing literature (Andrews et al., 2006; Beghein and Trampert, 2003; Deuss, 2008; Deuss et al., 2013; Durek and Romanowicz, 1999; He and Tromp, 1996; Irving and Deuss, 2011; Laske and Masters, 1999; Mäkinen et al., 2014), and 23 modes not present in both REM and DR were discarded ($_1S_7$, $_2S_2$, $_3S_8$, $_5S_3$, $_6S_0$, $_6S_1$, $_6S_2$, $_7S_3$, $_7S_4$, $_7S_5$, $_{10}S_2$, $_{11}S_1$, $_{13}S_6$, $_{15}S_7$, $_{17}S_8$, $_{18}S_2$, $_{18}S_4$, $_{18}S_6$, $_{20}S_2$, $_{20}S_4$, $_{21}S_8$, $_{22}S_2$, $_{27}S_1$,). Remaining modes were assessed on their theoretical proportion of total sensitivity within the IC. This resulted in the following 41 modes, used in the present study:

$_1S_0$, $_2S_0$, $_2S_3$, $_3S_0$, $_3S_1$, $_3S_2$, $_4S_0$, $_5S_3$, $_6S_3$, $_7S_5$, $_8S_1$, $_8S_5$, $_9S_2$, $_9S_3$, $_9S_4$, $_{11}S_4$, $_{11}S_5$, $_{11}S_6$, $_{13}S_1$, $_{13}S_2$, $_{13}S_3$, $_{14}S_4$, $_{15}S_3$, $_{15}S_4$, $_{16}S_5$, $_{16}S_6$, $_{16}S_7$, $_{17}S_1$, $_{18}S_3$, $_{18}S_4$, $_{20}S_1$, $_{20}S_5$, $_{21}S_6$, $_{21}S_7$, $_{22}S_1$, $_{23}S_4$, $_{23}S_5$, $_{25}S_1$, $_{25}S_2$, $_{27}S_2$.

2.3. Mode classification

Each normal mode presents different frequency sensitivity kernels for each of the three elastic parameters (V_s, V_p, ρ) as a function of depth (Fig. 1).

Here, we group modes into 3 groups: "radial", "PKIKP-equivalent" or "PKJKP-equivalent" (Fig. 2). The latter two were separated according to the relative proportion of IC sensitivity to V_p and V_s.

2.4. Observational uncertainty

Accounting for observational uncertainty is important for assessing the physical interpretability of our results. However, published uncertainty values vary by orders of magnitude between different center-frequency catalogues. Therefore, we make a conservative approach by using the measurement variability, i.e. the differences (Δω) between observed center-frequencies in our chosen catalogues, REM and DR (Fig. 3), as an estimation of uncertainty. The corresponding uncertainty estimates are on average an order of magnitude larger than the published estimates in DR, though still significantly smaller than those of REM (Supplementary Fig. S1). Each mode is then assigned a grouping based on the magnitude of the corresponding difference. The estimated observation uncertainty, σ_{est}, is calculated as the median difference, $\overline{\Delta\omega}$, scaled by a factor assigned to each group, G

$$\sigma_{est} = G\overline{\Delta\omega} \quad (1)$$

Here we assign low (Group 1), intermediate (Group 2) and high Δω (Group 3) modes scaling factors of 1, 2 and 3 respectively. However, we

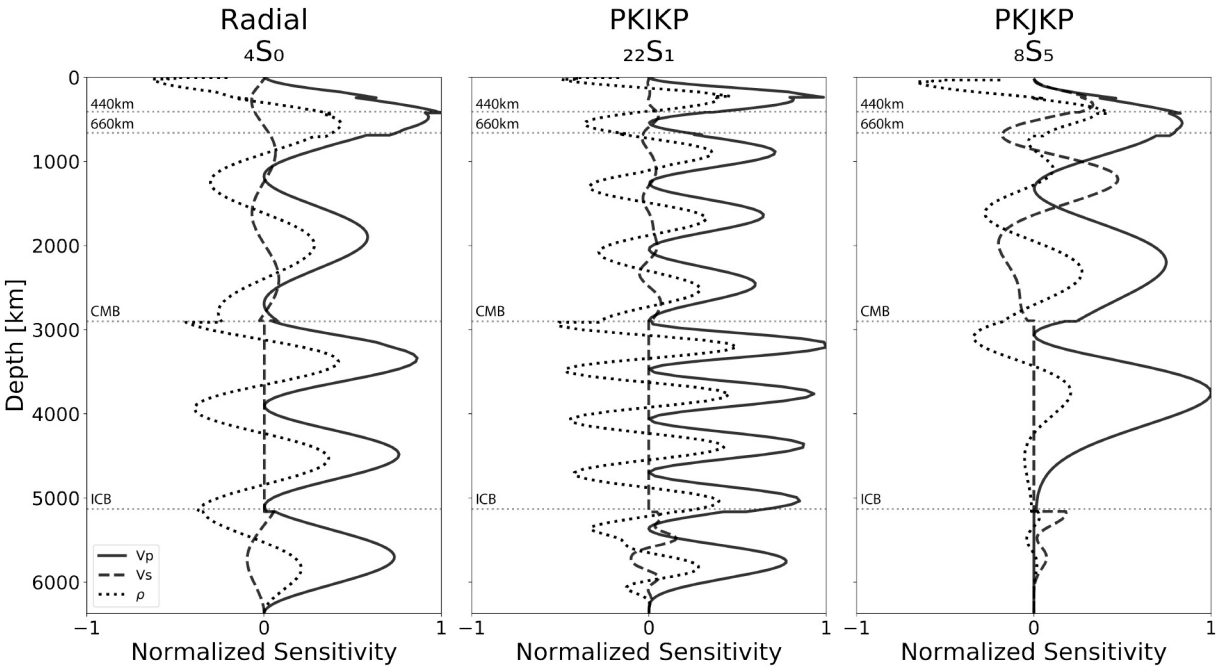

Fig. 1. Normalized sensitivity kernels of IC-sensitive modes: $_4S_0$, $_{22}S_1$, $_8S_5$ (calculated in PREM), showing the relative predicted center-frequency shift expected for a perturbation in the model in V_p, V_s and ρ, respectively.

note that the choice of these factors has little effect on results within reasonable limits (results are stable until the denominator of the cost function varies by a factor of ~750 between group 1 and 3).

2.5. Background models

To explore the effects of assumed mantle and OC structure on recovered IC structure, we utilize two background models, PREM (Dziewonski and Anderson, 1981) and NREM (Moulik, personal correspondence, 2019 based on Moulik and Ekström, 2016). Both models were independently constructed to fit normal mode observations, using different datasets and assumptions. These models were used here to provide all elastic and anelastic structure outside of the IC, and for IC quality factors.

3. Methodology

We consider average, homogeneous inner core models, ignoring any depth-dependence in V_p, V_s and ρ. Since these parameters vary slowly within the IC, this is a good first-order approximation of IC structure and helps mitigate computational limitations. We explore this 3-dimensional parameter-space via a grid-search, following the procedure outlined in Fig. 4.

Within some a-priori bounds, containing all proposed seismological and experimental estimates, we generated a suite of 1D models, each composed of a homogeneous IC in V_p, V_s and ρ, overlain by a published background model (e.g. PREM or NREM). IC quality factors were also fixed to those of the background model, as preliminary testing showed multiple orders of magnitude higher sensitivity to changes in V_p, V_s and

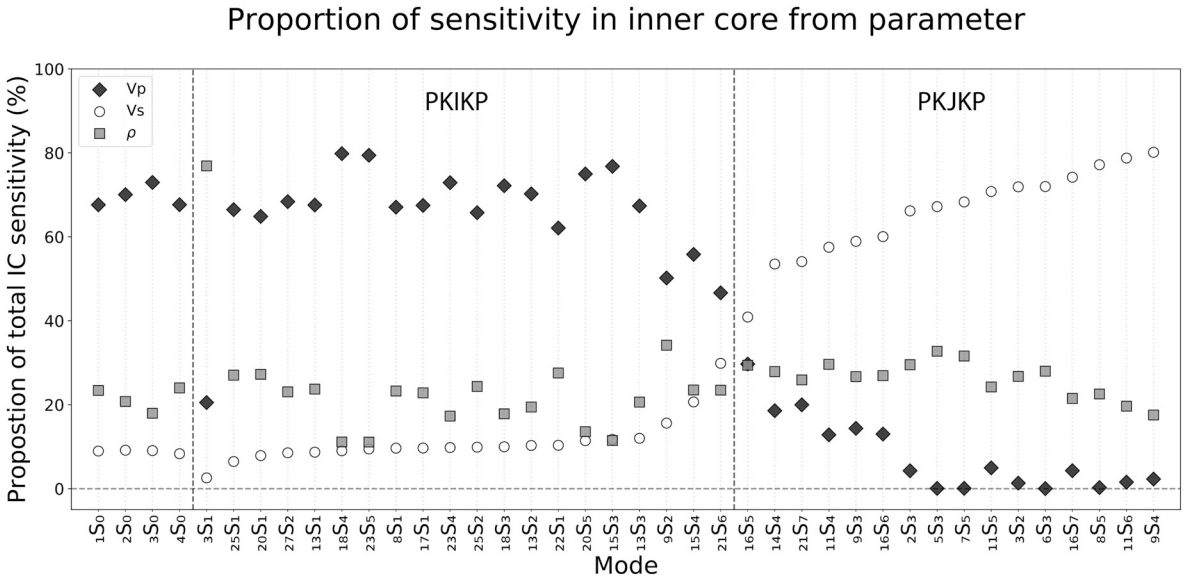

Fig. 2. The relative proportion of IC-sensitivity to V_p, V_s and ρ for each mode considered. Values represent the percentage of the sum of the integrals over depth in the IC of each parameter's sensitivity kernel (Fig. 1). Dashed vertical lines separate modes characterized as radial, PKIKP and PKJKP.

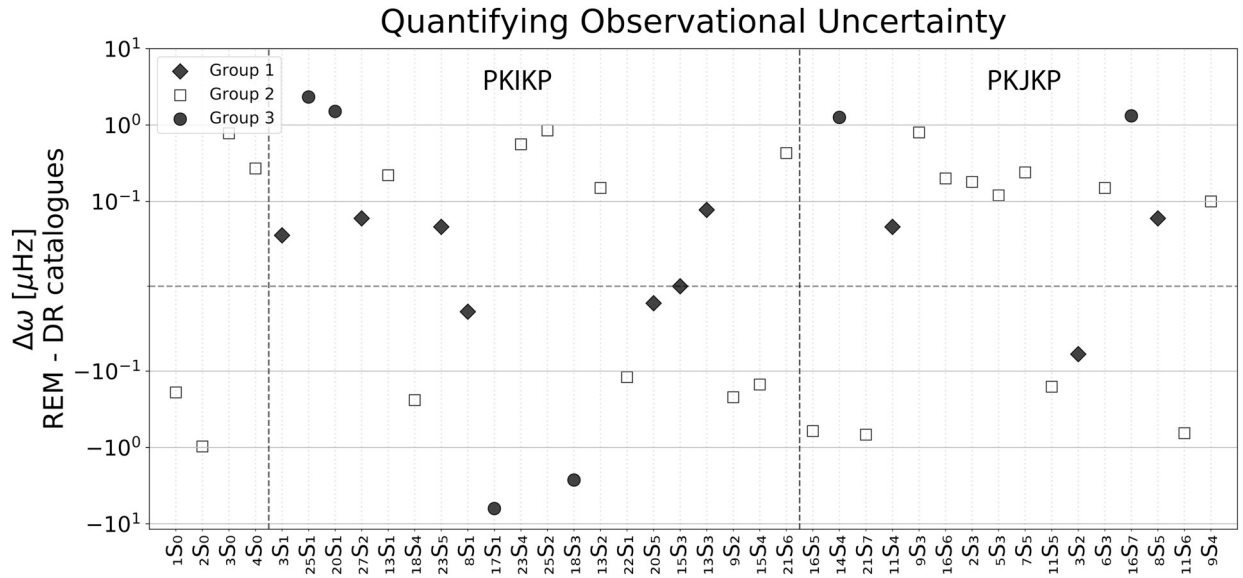

Fig. 3. Observational uncertainty grouping. For each mode the signed difference in observed frequency between REM and DR is plotted (Δω). Different symbols denote the corresponding uncertainty grouping. e.g. circles are Group 3, the observations with poorest agreement between catalogues, resulting in a where $\bar{\sigma}$ is the median Δω across all modes (0.21 μHz). Horizontal broken lines separate the different groups.

ρ, than in Qκ or Qμ. This also limited the dimensions of the problem, further reducing computations. Parameter spacing within the grid search was kept constant across runs, with velocities and ρ varying in increments of 10 m/s and 10 kg/m^3, respectively.

For each model, normal mode center-frequencies were predicted for our selection of IC-sensitive normal modes using MINOS (Woodhouse, 1998). A sum of squared differences was computed against a catalog of observed center-frequencies and a cost assigned to each model (Eq. (2)).

$$\phi = \sum_{i=1}^{N} \frac{(\omega_i^{obs} - \omega_i^{calc})^2}{\sigma_i^2} \frac{1}{C_i} \quad (2)$$

Here N is the total number of modes, and ω denotes mode frequency. Each mode's contribution to the cost function is weighted by two factors, observational error, σ_i, and mode character, $\mathbf{C_i}$ (e.g. Fig. 1, PKIKP, PKJKP or radial mode).

We consider two different C-weighting schemes: (a) where all modes have equal weights – "**all-equal**" (C_i = N for all i's) and the other and (b) "**PPR**", which accounts for the different number of modes in each mode group (PKIKP,PKJKP, radial). In scheme (b) $C_i = 3M_i$ where M_i is the number of modes within i-th mode's mode group. Normalizing by sensitivity groupings can help improve the strength of constraints provided by IC-sensitive normal modes on bulk IC parameters (Deuss, 2008).

The methodology outlined (Fig. 4) was repeated 16 times, for each permutation of 1) our two C-weighting schemes: PPR and all-equal 2) different observational catalogues: REM and DR 3) different background models: PREM and NREM and 4) different σ values: with our estimation of observation uncertainty $\sigma = \sigma_{est}$, as described earlier, and using normalization by observed frequency, $\sigma = \omega_{obs}$. The latter ensures that differences are not unintentionally upweighted for high frequency modes i.e. a 1% difference will be weighted the same at all frequencies.

4. Results

The bulk IC velocities are found to be consistent across all 16 runs (Table 1). V_p values vary between 11,160–11,180 m/s, with a standard deviation of just 8 m/s, and are in good agreement with Deuss's proposed 2008 value (11,150 m/s) as well as PREM's IC average (11,183 m/s). V_s values are similarly well-constrained (3560–3590 m/s with a standard deviation of 10 m/s) and exhibit a minor reduction of ~1% with respect to PREM (34 m/s) and are in better agreement with Deuss (3550 m/s). N.B. Unless otherwise stated, reference averages computed in the reference PREM model are linear averages, as volumetric averages overly emphasizes the outermost inner core's effect on modal frequencies. While we also acknowledge linear averages underemphasize this contribution, we believe the context of our results are largely independent of this decision. Though for clarity, volumetric averages are marked alongside the linear averages in Fig. 5.

Our results provide looser constraints on IC density, with values ranging from 12,720–12,880 kg/m^3(+/− 54 kg/m^3) (Fig. 5). Still, the results show a reduction in average IC density with respect to PREM on

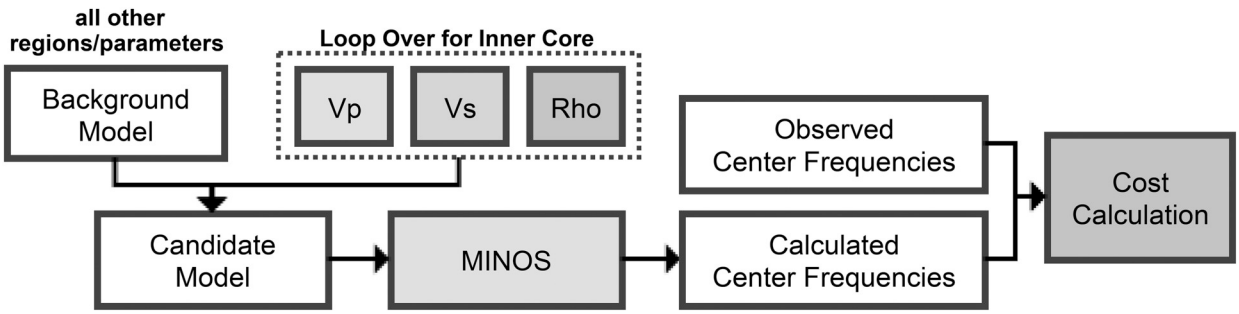

Fig. 4. Parameter-space search methodology. A suite of models is generated, each with a unique homogeneous inner core in V_p, V_s and ρ. All other parameters and regions are set to the background model. For each of these unique models, center-frequencies are calculated via MINOS and the cost function evaluated (Eq. (2)).

Table 1
The homogeneous IC parameters associated with the lowest cost models for each of the 8 runs using NREM in the mantle and OC (top) and those using PREM (bottom). Mean and standard deviation values are also shown for each subset, as are PREM's linear averages, maximum and minimum values for comparison. A reduction in V_s and ρ with respect to PREM can be seen across all runs and is particularly pronounced in the runs with NREM in the outer core and mantle. The distribution of these models can be visualized in Fig. 5.

Background model	NREM												
Observations	DR				REM								
C-weighting	PKIKP:PKJKP:radial		All-equal		PKIKP:PKJKP:radial		All-equal						
σ-Weighting	ω_{obs}	σ_{est}	ω_{obs}	σ_{est}	ω_{obs}	σ_{est}	ω_{obs}	σ_{est}	Mean	S.D.	PREM min.	PREM max.	PREM's linear average
Vp	11,180	11,170	11,170	11,160	11,180	11,160	11,170	11,160	11,169	8	11,028	11,262	11,183
Vs	3,570	3,570	3,570	3,570	3,560	3,570	3,570	3,570	3,569	4	3,504	3,668	3,612
ρ	12,760	12,820	12,750	12,790	12,720	12,790	12,720	12,770	12,765	35	12,764	13,089	12,979
Model name	A	B	C	D	E	F	G	H					

Background model	PREM												
Observations	DR				REM								
C-weighting	PKIKP:PKJKP:radial		All-equal		PKIKP:PKJKP:radial		All-equal						
σ-Weighting	ω_{obs}	σ_{est}	ω_{obs}	σ_{est}	ω_{obs}	σ_{est}	ω_{obs}	σ_{est}	Mean	S.D.	PREM min.	PREM max.	PREM's linear average
Vp	11,170	11,170	11,160	11,160	11,180	11,170	11,160	11,160	11,166	7	11,028	11,262	11,183
Vs	3,580	3,590	3,590	3,590	3,580	3,590	3,590	3,590	3,588	5	3,504	3,668	3,612
ρ	12,810	12,880	12,830	12,880	12,750	12,870	12,800	12,860	12,835	46	12,764	13,089	12,979
Model name	I	J	K	L	M	N	O	P					

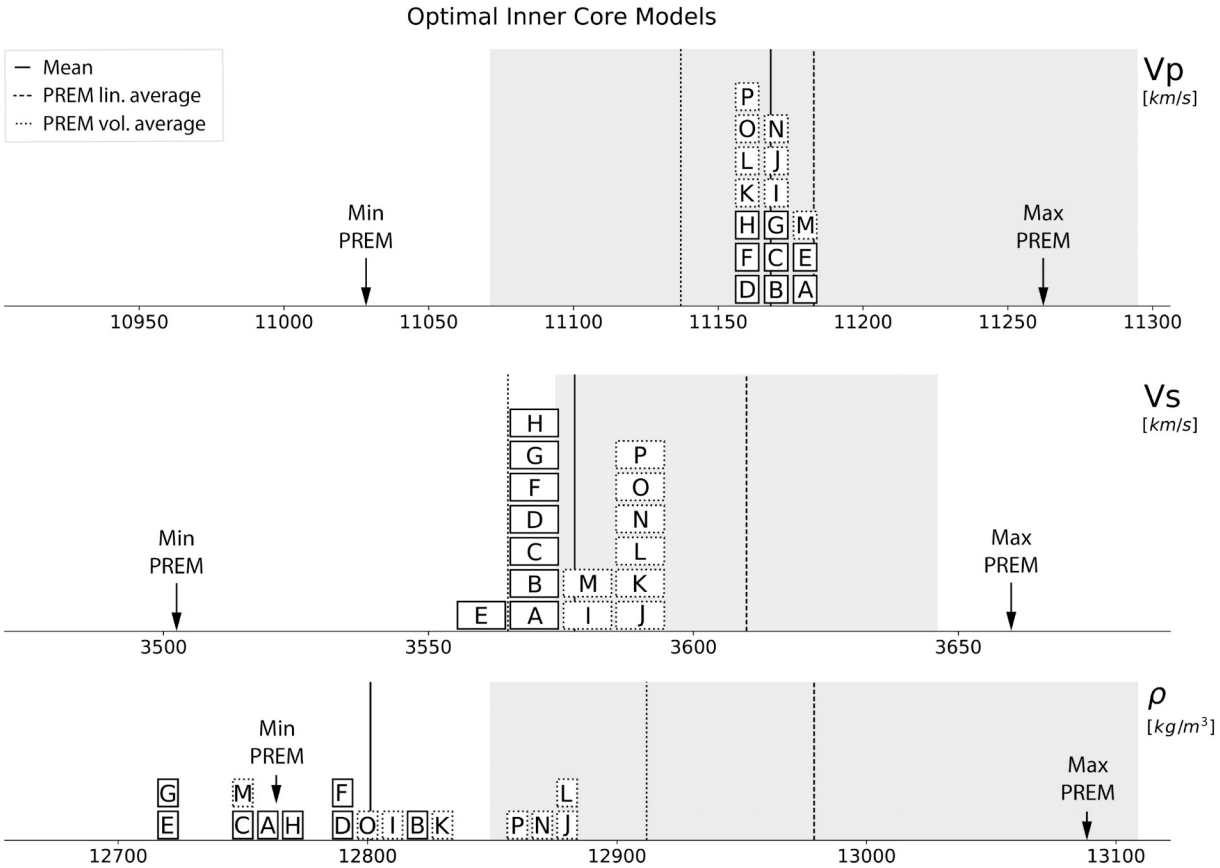

Fig. 5. Histogram showing the distribution of parameters in the 16 best-fitting models. Letters correspond to the final letter of the model names shown in Table 1. The grey box represents a 1% variation in PREM's linear average for each parameter. Models using NREM's mantle and outer core (solid outlines) are distributed towards lower values in V_s and ρ than PREM's (dotted outlines), while there is no clear difference between the two background models in V_p.

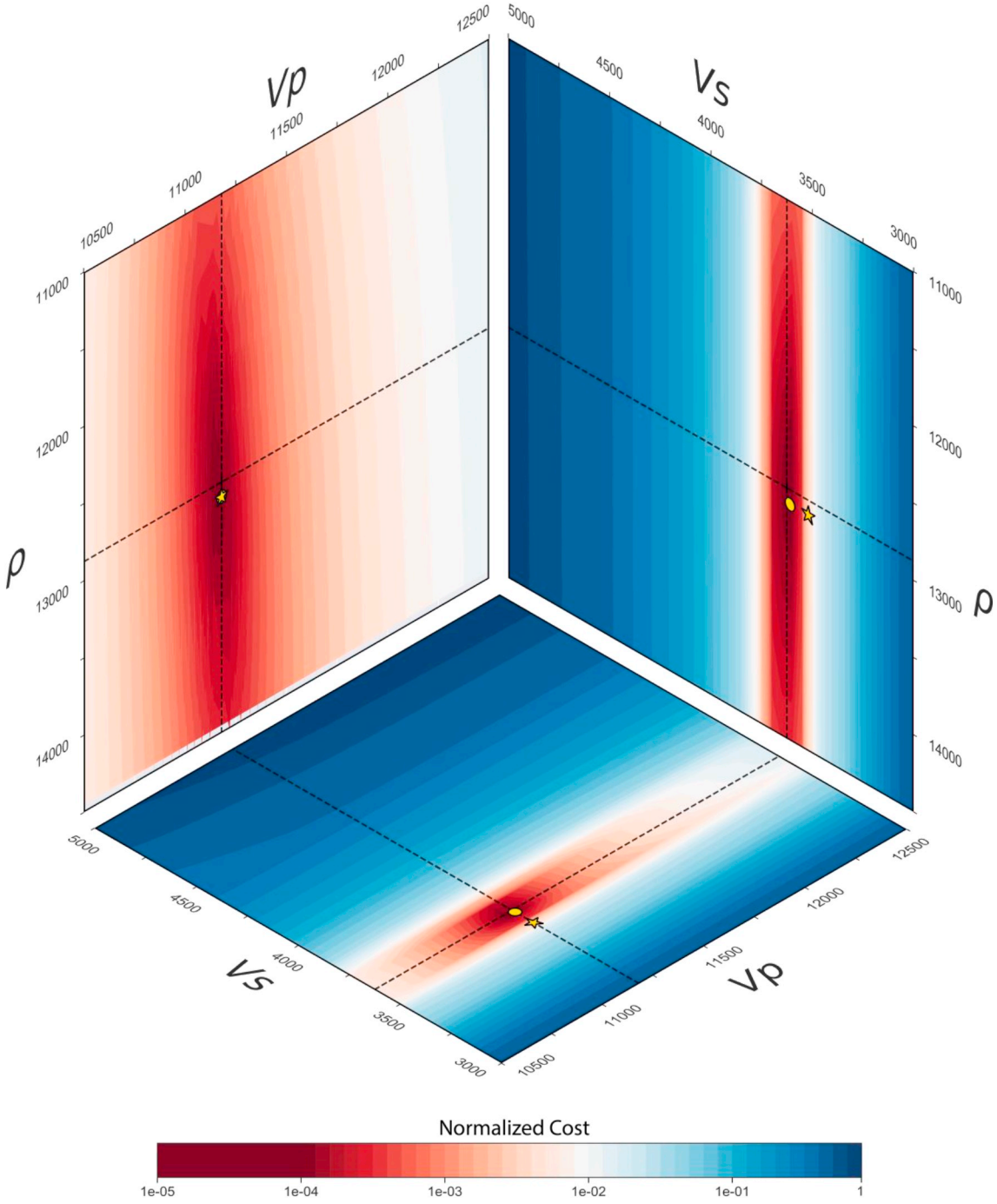

Fig. 6. The normalized cost function (Eq. (1)) across the parameter space (Run A, in Table 1). Dashed lines represent where the three panes intersect, and the lines cross at the minima. The location of a model with -2.5% V_s in the inner core is marked with a star, showing an increase in cost of 2.5 orders of magnitude, with respect to the best-fitting model, while PREM's average IC values (marked with a yellow circle; note: circle and star overlap in ρ/Vp space) are associated with roughly 157% the cost of the best fitting model. V_s exhibits the steepest gradient in the cost function, indicating it is the best constrained parameter when holding run parameters such as the background model, and dataset, constant. V_p is still well-constrained and in very good agreement with PREM, V_s favors a minor reduction (1.1%) with respect to PREM, while the best-fitting density is ~219 kg/m^3 lower than PREM (~1.7%). The location of a model with -2.5% V_s in the inner core is marked, showing an increase in cost of 2.5 orders of magnitude, with respect to the best-fitting model. (For interpretation of the references to colour in this figure legend, the reader is referred to the web version of this article.)

the order of 1.3%, with a mean density of 12,801 kg/m^3.

The level of constraints on each of these variables can be seen in a different way by visualizing the cost function across the parameter-space (Fig. 6). The cost function exhibits a steeper gradient and thus greater sensitivity in V_s while showing less stringent constraints on V_p and relatively weak constraints on ρ. Still, the V_p remains the closest to PREM.

5. Discussion

We have shown that the recent normal mode center-frequency catalogues considered provide constraints on bulk IC V_p, V_s and ρ that are largely independent of the dataset, data uncertainty, and to some extent on the choice of reference OC and mantle model.

Additionally, to explore the effects of a deviation from PREM's IC

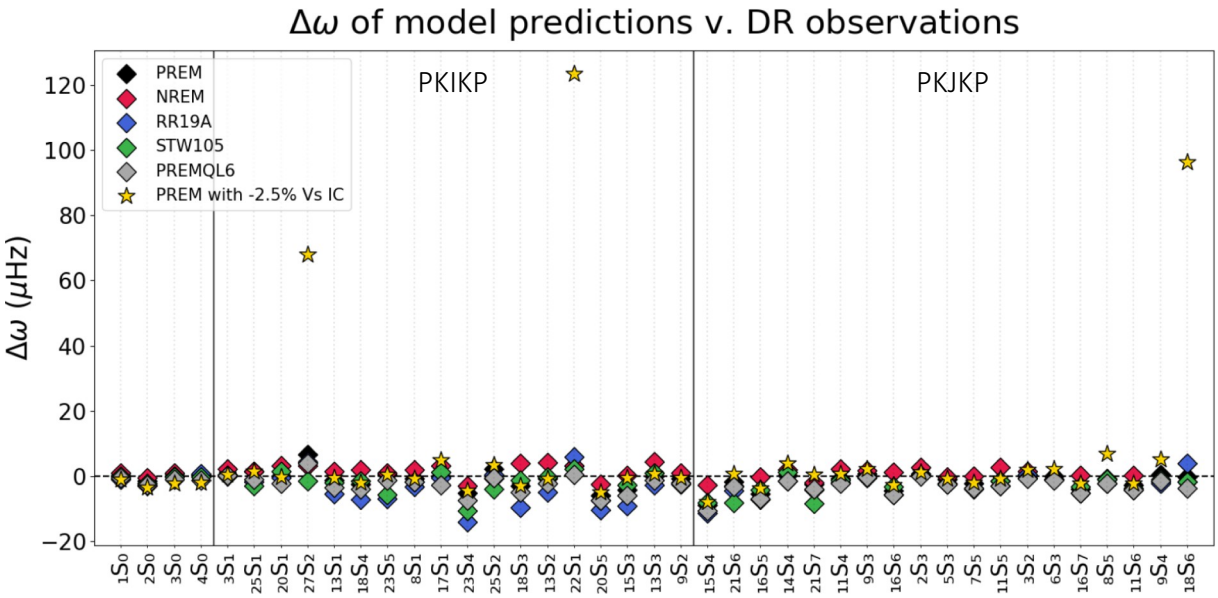

Fig. 7. Comparison of center-frequency predictions to DR observations. For each IC-sensitive mode the difference between its predicted Eigenfrequencies and observed (DR) Eigenfrequencies is shown. Models include: PREM, NREM, PREMQL6 (Durek and Ekström, 1996; Dziewonski and Anderson, 1981), STW105 (Kustowski et al., 2008), and the best-fitting model from Fig. 6 – Model A. Notably, a reduction of 2.5% in IC shear velocity (stars) is associated with increased misfits for many IC-senstive modes, particularly $_8S_5$, $_9S_4$, $_{18}S_6$, $_{22}S_1$ and $_{27}S_2$. Note, $_{18}S_6$ (far right) was not used to generate our models as it was not present in REM. However, it is a PKJKP-like mode with high IC-sensitivity to V_s. Please note, all models are depth dependent in the IC other than RR19A (Model A – Table 1) which has a homogeneous IC.

radius, proposed by a recent normal mode study (de Wit et al., 2014), we performed tests (not shown), finding results were insensitive to changes in IC radius within reasonable bounds (± 20 km). We did not explicitly explore the effect of inner core anisotropy (Woodhouse et al., 1986) on the center frequencies, ignoring the effects of cross-coupling due to IC anisotropy and 3D mantle structure in our simulations. However, in contrast to the construction of PREM, developed before the discovery of anomalous mode splitting, recent normal mode measurements are based on extracting the constant, “00” term in a spherical harmonics expansion of mode splitting functions, while the anisotropy signature is in the higher order terms. Also, since we compare the results based on two different catalogues, constructed from measurements by different authors, using different techniques, we may assume that any hidden effect of anisotropy may be reflected in the conservative errors we have assigned to the data.

We note that a recently proposed reduction in V_s of 2.5% in the IC, keeping V_p and ρ fixed at the PREM values (Tkalčić and Pham, 2018), is incompatible with normal mode observations, exhibiting orders of magnitude higher cost than best-fitting models (Fig. 6). Additionally, while most mode center-frequencies in our catalog are arguably fit no worse than by other existing models (Fig. 7), several modes stand out: predictions for modes $_{27}S_2$, $_{22}S_1$ and $_{18}S_6$ are particularly poor (considerably outside observational uncertainty, e.g. Fig. 3), and predictions for at least two additional PKJKP modes ($_8S_5$ and $_9S_4$) are also outside of error bounds. The effects of this V_s perturbation vary (Fig. 7) across modes with similar IC sensitivity proportions (Fig. 2), emphasizing the importance of parameter trade-offs and the need for a simultaneous search. While Tkalčić and Pham (2018) did additionally explore V_p and Qμ, these where separate steps keeping other parameters fixed while they varied, leaving trade-off effects unexplored.

Density values are less well-constrained than velocities. However, our results consistently favor a significant reduction in average density with respect to PREM (0.7–1.9%). This reduction may result from differences in the observed center-frequencies in our catalog, compared to those used in the construction of PREM. It may also result from the additional constraints used in PREM, such as the Adam-Williamson equation, and Earth's Mass and moment of inertia. Clearly, normal mode observations alone offer poorer constraints for IC density than for other parameters (Fig. 6), and while mass and moment of inertia are well known, these parameters do not help to constrain IC density, given uncertainty in shallower density structure (Irving et al., 2018). We note that slightly lower V_s and ρ values are obtained when fixing structure in the mantle and outer core to that in NREM (Fig. 5), which presumably is an improved 1D model over PREM. Considering the values obtained with NREM, the data require a reduction of 1.1% in V_s and 1.3% in ρ with respect to PREM.

Finally, we acknowledge that mode sensitivity to V_p, V_s and ρ reduces to zero at the Earth's center (Fig. 1). As a result, on average, normal modes have greater sensitivity at shallower depths, so that best-fitting bulk IC parameters may be more representative of the top part of the IC.

It is clear that normal modes favor a reduction in IC density with respect to PREM, though the magnitude of such a reduction is weakly constrained (Fig. 5/6). This reduction may have important implications for our understanding of the driving mechanism of the geodynamo. When considered with PREM's outer core, best-fitting models reduce the magnitude of the density jump (Δρ) at the ICB in PREM (603 kg/m^3) by between 89 and 242 kg/m^3. This is significant given the magnitude of the density jump due to solidification alone can be estimated to be about 210 kg/m^3 (Alfè et al., 2000). As such, our density reduction may reduce the jump associated with light element partitioning by over half, having significant implications for the ability of that mechanism to power the geodynamo. This issue is potentially compounded when considering the results of another recent mode study in the outer core (Irving et al., 2018), which favored an increase in average OC density. This would bring the mode-derived value close to the lower end of the values obtained from recent PKiKP/PcP amplitude ratio measurements, which span a range of 300 to 1200 kg/m^3 for Δρ (e.g. Cao and Romanowicz, 2004; Koper and Dombrovskaya, 2005; Shen et al., 2016; Tkalčić et al., 2009; Waszek and Deuss, 2015), although the higher values obtained in some of these studies may be due to amplification due to focusing by topography on the inner-core boundary.

While we present results for the simplest possible parameterization of IC parameters, attempts were made to explore depth dependence via

both linear and quadratic forms. However, when using center-frequencies alone, the higher order terms – and so the gradients – were unstable and highly dependent on the choice of grid-search points for the zeroth order term. Introduction of additional independent constraints from mineral physics, such as a Birch type V_p-ρ relation (Birch, 1961; Sakamaki et al., 2016), or assuming hydrostatic equilibrium is necessary to stabilize results and reduce the dimensions of the problem.

Overall, our results reaffirm PREM's average IC V_p, suggest a slight reduction in V_s (~1%) and a larger reduction in density (~0.7–1.9%), while acknowledging limitations in constraining IC ρ based on normal mode center-frequency data alone.

6. Conclusions

Using a catalog of well-characterized IC-sensitive normal mode center-frequencies based on recent measurements, and exploring variations in average V_s, V_p and ρ in the IC simultaneously, we have shown that IC velocities are well-constrained by these data, independent of choice of: dataset, mantle model, data uncertainty and IC radius. We find V_p is in good agreement with PREM and a minor reduction in V_s with respect to PREM is favored (~1%). We show that a more significant reduction of 2.5% in V_s, while fixing ρ to PREM as proposed by Tkalčić and Pham (2018), is incompatible with normal mode center-frequency observations. Meanwhile, normal mode center-frequency data favor a reduction in average ρ in the IC of between 0.7 and 1.7%, although data-sensitivity to ρ is significantly lower than to V_p and V_s.

While normal modes alone struggle to constrain the elastic parameters' depth-dependence within the IC, these best-fitting average values and their associated standard deviations may be useful for laboratory and ab-initio studies aiming at constraining IC composition. If confirmed, the slight density reduction favored by our models may have important implications for the energy available to power the geodynamo, potentially reducing the magnitude of the ICB density jump associated with light element partitioning by over half, compared to the PREM value.

Supplementary data to this article can be found online at https://doi.org/10.1016/j.pepi.2019.106310.

Acknowledgements

We thank Gabi Laske for putting together the REM website (https://igppweb.ucsd.edu/~gabi/rem.html) and Pritwiraj Moulik for sharing his new mantle model in advance of publication. This work was supported by NSF grants EAR-1345103 and EAR-1464014.

References

Alfè, D., Kresse, G., Gillan, M.J., 2000. Structure and dynamics of liquid iron under Earth's core conditions. Phys. Rev. B 61, 132–142. https://doi.org/10.1103/physrevb.61.132.

Andrews, J., Deuss, A., Woodhouse, J., 2006. Coupled normal-mode sensitivity to inner-core shear velocity and attenuation. Geophys. J. Int. 167, 204–212. https://doi.org/10.1111/j.1365-246x.2006.03022.x.

Antonangeli, D., Siebert, J., Badro, J., Farber, D.L., Fiquet, G., Morard, G., Ryerson, F.J., 2010. Composition of the Earth's inner core from high-pressure sound velocity measurements in Fe–Ni–Si alloys. Earth Planet. Sci. Lett. 295, 292–296. https://doi.org/10.1016/j.epsl.2010.04.018.

Bazhanova, Z.G., Oganov, A.R., Gianola, O., 2012. Fe–C and Fe–H systems at pressures of the Earth's inner core. Physics-Uspekhi 55, 489–497. https://doi.org/10.3367/ufne.0182.201205c.0521.

Beghein, C., Trampert, J., 2003. Robust normal mode constraints on inner-core anisotropy from model space search. Science. 299, 552–555. https://doi.org/10.1126/science.1078159.

Belonoshko, A.B., Skorodumova, N.V., Davis, S., Osiptsov, A.N., Rosengren, A., Johansson, B., 2007. Origin of the low rigidity of the Earth's inner core. Science. 316, 1603–1605. https://doi.org/10.1126/science.1141374.

Birch, F., 1952. Elasticity and constitution of the Earth's interior. J. Geophys. Res. 57, 227–286. https://doi.org/10.1029/jz057i002p00227.

Birch, F., 1961. The velocity of compressional waves in rocks to 10 kilobars, part 2. J. Geophys. Res. 66, 2199–2224. https://doi.org/10.1029/sp026p0091.

Birch, F., 1964. Density and composition of mantle and core. J. Geophys. Res. 69, 4377–4388. https://doi.org/10.1029/jz069i020p04377.

Cao, A., Masson, Romanowicz, B., 2005. An observation of PKJKP: inferences on inner core shear properties. Science. 308, 1453–1455. https://doi.org/10.1126/science.1109134.

Cao, A., Romanowicz, B., 2004. Constraints on density and shear velocity contrasts at the inner core boundary. Geophys. J. Int. 157, 1146–1151. https://doi.org/10.1111/j.1365-246x.2004.02330.x.

Caracas, R., 2015. The influence of hydrogen on the seismic properties of solid iron. Geophys. Res. Lett. 42, 3780–3785. https://doi.org/10.1002/2015gl063478.

de Wit, R.W.L., Käufl, P.J., Valentine, A.P., Trampert, J., 2014. Bayesian inversion of free oscillations for Earth's radial (an)elastic structure. Phys. Earth Planet. Inter. 237, 1–17. https://doi.org/10.1016/j.pepi.2014.09.004.

Deuss, A., 2008. Normal mode constraints on shear and compressional wave velocity of the Earth's inner core. Earth Planet. Sci. Lett. 268, 364–375. https://doi.org/10.1016/j.epsl.2008.01.029.

Deuss, A., Woodhouse, J.H., Paulssen, H., Trampert, J., 2000. The observation of inner core shear waves. Geophys. J. Int. 142, 67–73. https://doi.org/10.1046/j.1365-246x.2000.00147.x.

Deuss, A., Ritsema, J., van Heijst, H., 2013. A new catalogue of normal-mode splitting function measurements up to 10 mHz. Geophys. J. Int. 193, 920–937. https://doi.org/10.1093/gji/ggt010.

Durek, J.J., Ekström, G., 1996. A radial model of anelasticity consistent with long-period surface-wave attenuation. Bull. Seismol. Soc. Am. 86, 144–158.

Durek, J.J., Romanowicz, B., 1999. Inner core anisotropy inferred by direct inversion of normal mode spectra. Geophys. J. Int. 139, 599–622. https://doi.org/10.1046/j.1365-246x.1999.00961.x.

Dziewonski, A.M., Anderson, D.L., 1981. Preliminary reference earth model. Phys. Earth Planet. Inter. 25, 297–356. https://doi.org/10.1016/0031-9201(81)90046-7.

Dziewonski, A.M., Gilbert, F., 1971. Solidity of the inner core of the earth inferred from normal mode observations. Nature 234, 465–466. https://doi.org/10.1038/234465a0.

Gubbins, D., Masters, T.G., Jacobs, J.A., 1979. Thermal evolution of the Earth's core. Geophys. J. Int. 59, 57–99. https://doi.org/10.1111/j.1365-246x.1979.tb02553.x.

He, X., Tromp, J., 1996. Normal-mode constraints on the structure of the Earth. J. Geophys. Res. Solid Earth 101, 20053–20082. https://doi.org/10.1029/96jb01783.

Hirose, K., Morard, G., Sinmyo, R., Umemoto, K., Hernlund, J., Helffrich, G., Labrosse, S., 2017. Crystallization of silicon dioxide and compositional evolution of the Earth's core. Nature 543, 99–102. https://doi.org/10.1038/nature21367.

Irving, J.C.E., Deuss, A., 2011. Stratified anisotropic structure at the top of Earth's inner core: a normal mode study. Phys. Earth Planet. Inter. 186, 59–69. https://doi.org/10.1016/j.pepi.2011.03.003.

Irving, J.C.E., Cottaar, S., Lekić, V., 2018. Seismically determined elastic parameters for Earth's outer core. Sci. Adv. 4, eaar2538. https://doi.org/10.1126/sciadv.aar2538.

Jephcoat, A., Olson, P., 1987. Is the inner core of the Earth pure iron? Nature 325, 332–335. https://doi.org/10.1038/325332a0.

Julian, B.R., Davies, D., Sheppard, R.M., 1972. PKJKP. Nature 235, 317–318. https://doi.org/10.1038/235317a0.

Koper, K.D., Dombrovskaya, M., 2005. Seismic properties of the inner core boundary from PKiKP/P amplitude ratios. Earth Planet. Sci. Lett. 237, 680–694. https://doi.org/10.1016/j.epsl.2005.07.013.

Kustowski, B., Ekström, G., Dziewoński, A.M., 2008. Anisotropic shear-wave velocity structure of the earth's mantle: a global model. J. Geophys. Res. Solid Earth 113, 1–23. https://doi.org/10.1029/2007JB005169.

Laske, G., Masters, G., 1999. Limits on differential rotation of the inner core from an analysis of the Earth's free oscillations. Nature 402, 66–69. https://doi.org/10.1038/47011.

Lehmann, I., 1936. P'. Bur. Centr. Seism. Internat. Ser. A 14.

Li, Y., Vočadlo, L., Brodholt, J.P., 2018. The elastic properties of hcp-Fe alloys under the conditions of the Earth's inner core. Earth Planet. Sci. Lett. 493, 118–127. https://doi.org/10.1016/j.epsl.2018.04.013.

Loper, D.E., 1978. Some thermal consequences of a gravitationally powered dynamo. J. Geophys. Res. Solid Earth 83, 5961–5970. https://doi.org/10.1029/jb083ib12p05961.

Mäkinen, A.M., Deuss, A., Redfern, S.A.T., 2014. Anisotropy of Earth's inner core intrinsic attenuation from seismic normal mode models. Earth Planet. Sci. Lett. 404, 354–364. https://doi.org/10.1016/j.epsl.2014.08.009.

Martorell, B., Vocadlo, L., Brodholt, J., Wood, I.G., 2013. Strong premelting effect in the elastic properties of hcp-Fe under inner-core conditions. Science. 342, 466–468. https://doi.org/10.1126/science.1243651.

Masters, G., Gubbins, D., 2003. On the resolution of density within the Earth. Phys. Earth Planet. Inter. 140, 159–167. https://doi.org/10.1016/j.pepi.2003.07.008.

Moulik, P., Ekström, G., 2016. The relationships between large-scale variations in shear velocity, density, and compressional velocity in the Earth's mantle. J. Geophys. Res. Solid Earth 121, 2737–2771. https://doi.org/10.1002/2015jb012679.

Okal, E.A., Cansi, Y., 1998. Detection of PKJKP at intermediate periods by progressive multi-channel correlation. Earth Planet. Sci. Lett. 164, 23–30. https://doi.org/10.1016/s0012-821x(98)00210-6.

Oldham, R.D., 1906. The constitution of the interior of the Earth, as revealed by earthquakes. Q. J. Geol. Soc. 62, 456–475. https://doi.org/10.1144/gsl.jgs.1906.062.01-04.21.

Poirier, J.-P., 1994. Light elements in the Earth's outer core: a critical review. Phys. Earth Planet. Inter. 85, 319–337. https://doi.org/10.1016/0031-9201(94)90120-1.

Reference Earth Model. https://igppweb.ucsd.edu/~gabi/rem.dir/surface/smodes.list, Accessed date: 1 February 2017.

Roult, G., Roch, J., Clévédé, E., 2010. Observation of split modes from the 26th December 2004 Sumatra-Andaman mega-event. Phys. Earth Planet. Inter. 179, 45–59. https://

doi.org/10.1016/j.pepi.2010.01.001.
Sakamaki, T., Ohtani, E., Fukui, H., Kamada, S., Takahashi, S., Sakairi, T., Takahata, A., Sakai, T., Tsutsui, S., Ishikawa, D., et al., 2016. Constraints on Earth's inner core composition inferred from measurements of the sound velocity of hcp-iron in extreme conditions. Sci. Adv. 2, e1500802. https://doi.org/10.1126/sciadv.1500802.
Shearer, P.M., Rychert, C.A., Liu, Q., 2011. On the visibility of the inner-core shear wave phase PKJKP at long periods. Geophys. J. Int. 185, 1379–1383. https://doi.org/10.1111/j.1365-246x.2011.05011.x.
Shen, Z., Ai, Y., He, Y., Jiang, M., 2016. Using pre-critical PKiKP–PcP phases to constrain the regional structures of the inner core boundary beneath East Asia. Phys. Earth Planet. Inter. 252, 37–48. https://doi.org/10.1016/j.pepi.2016.01.001.
Tagawa, S., Ohta, K., Hirose, K., Kato, C., Ohishi, Y., 2016. Compression of Fe-Si-H alloys to core pressures. Geophys. Res. Lett. 43, 3686–3692. https://doi.org/10.1002/2016gl068848.
Tkalčić, H., Pham, T.S., 2018. Shear properties of Earth's inner core constrained by a detection of J waves in global correlation wavefield. Science. 362, 329–332. https://doi.org/10.1126/science.aau7649.
Tkalčić, H., Kennett, B.L.N., Cormier, V.F., 2009. On the inner-outer core density contrast from PKiKP/PcP amplitude ratios and uncertainties caused by seismic noise. Geophys. J. Int. 179, 425–443. https://doi.org/10.1111/j.1365-246x.2009.04294.x.
Vočadlo, L., 2007. Ab initio calculations of the elasticity of iron and iron alloys at inner core conditions: evidence for a partially molten inner core? Earth Planet. Sci. Lett. 254, 227–232. https://doi.org/10.1016/j.epsl.2006.09.046.
Waszek, L., Deuss, A., 2015. Anomalously strong observations of PKiKP/PcP amplitude ratios on a global scale. J. Geophys. Res. Solid Earth 120, 5175–5190. https://doi.org/10.1002/2015jb012038.
Woodhouse, J.H., 1998. The calculation of Eigenfrequencies and Eigenfunctions of the free oscillations of the Earth and the sun. Seismol. Algorithms 321–370.
Woodhouse, J.H., Giardini, D., Li, X.-D., 1986. Evidence for inner core anisotropy from free oscillations. Geophys. Res. Lett. 13, 1549–1552. https://doi.org/10.1029/gl013i013p01549.
Wookey, J., Helffrich, G., 2008. Inner-core shear-wave anisotropy and texture from an observation of PKJKP waves. Nature 454, 873–876. https://doi.org/10.1038/nature07131.